Arabian Journal of Chemistry (2021) **14**, 103134

King Saud University

Arabian Journal of Chemistry

www.ksu.edu.sa
www.sciencedirect.com

ORIGINAL ARTICLE

Synergistic surface basicity enhancement effect for doping of transition metals in nanocrystalline MgO as catalysts towards one pot Wittig reaction

Mansur Moulavi [a], Kaluram Kanade [b,*], Dinesh Amalnerkar [c,*], Amanullah Fatehmulla [d], Abdullah M. Aldhafiri [d,*], M. Aslam Manthrammel [e]

[a] *Department of Chemistry, PDEA's Annasaheb Waghire College, Otur, Pune 412409, India*
[b] *Annasaheb Awate Arts, Commerce, Hutatma Babu Genu Science College, Manchar, Pune 410503, India*
[c] *Department of Technology, Savitribai Phule Pune University, Pune 411007, India*
[d] *Department of Physics & Astronomy College of Science, P.O. Box 2455, King Saud University, Riyadh 11451, Saudi Arabia*
[e] *Department of Physics, College of Science, King Khalid University, P.O. Box 9004, Abha, Saudi Arabia*

Received 16 December 2020; accepted 17 March 2021
Available online 24 March 2021

KEYWORDS

Synergistic effect;
Surface basicity;
Wittig reaction;
Mn doped MgO;
Nanomaterials;
Heterogeneous catalyst

Abstract The syntheses of Cu, Fe and Mn doped nanocrystalline MgO was carried out using alkali leached hydrothermal technique. The synergistic effect of transition metals (Cu, Fe and Mn) doping, particle size and nano-scale morphology on surface basicity enhancement was established in one pot Wittig reaction. The doped and undoped nanocrystalline MgO catalysts are characterized by XRD, UV-DRS, FT-IR, FESEM, EDS and XPS techniques. XRD study revealed formation of pure cubic phase of undoped and up to 1 wt% Cu, Fe and Mn doped MgO. The FESEM photographs of transition metal doped MgO indicated the formation of prismatic hexagonal nano plates and nanosheets with thickness in the range 20–70 nm. The catalytic activity of synthesized catalysts was investigated in one pot Wittig reaction of benzaldehyde, triphenylphosphine and ethyl bromoacetate at room temperature in DMF solvent. The Mn doped nanocrystalline MgO catalyst shows 98% yield under optimized reaction conditions. Enhancement of surface basicity due to doping of Mn in MgO was ascertained by UV-DRS and XPS study. The characterization of Wittig product ethyl cinnamate was carried out using HR-MS, ^{1}H NMR, ^{13}C NMR. The ^{1}H NMR evaluates 95:5% E/Z ratio of ethyl cinnmate. Reported methodology is eco-friendly and easy to scale up.

* Corresponding authors.
E-mail addresses: kgkanade@yahoo.co.in (K. Kanade), dpa54@yahoo.co.in (D. Amalnerkar), adhafiri@ksu.edu.sa (A.M. Aldhafiri).
Peer review under responsibility of King Saud University.

ELSEVIER Production and hosting by Elsevier

1. Introduction

Organic synthesis by heterogeneous catalysis is a fascinating art (Leng et al., 2013). Among the heterogeneous catalysis, several base catalyzed C—C bond forming organic reactions such

https://doi.org/10.1016/j.arabjc.2021.103134
1878-5352

as Aldol condensation (Hattori, 2001), Knoenvengal condensation (Lucrecia et al., 2016), Claisen Schmidt condensation (Drexler and Amiridis, 2003), Biginilli reaction (Shinde et al., 2016) and coupling reactions (Gholinejad et al., 2016, 2018) are well known. These heterogeneous organic reactions are catalyzed by MgO, ZnO, CaO, SrO, and TiO_2 catalysts via a green chemical approach (Kunde et al., 2016). Among these solids, MgO is used as a base catalyst. It is very cheap, easily available and recyclable catalyst (Babaie and Sheibani, 2011). Wittig reaction is one of the stereo-selective methods for preparation of olefin from aldehydes or ketones (Nicolaou et al., 1997). This important C—C bond forming reaction generally comprises two steps under homogenous basic conditions using NaOH, KOH, $Ba(OH)_2$, alkoxides, hydrides (Taber and Nelson, 2006). It suffers from many drawbacks such as drastic reaction conditions, contamination of products and excessively strong basic conditions. Thus, it requires huge amount of solvent for purification and vice versa unwanted separation. To overcome this, Wittig reaction can be made to operate in one pot without isolation of intermediate phosphonium salt and phosphorus ylide under heterogeneous mild reaction condition using nanocrystalline MgO. However, this heterogeneous basic condition requires longer reaction time (Moison et al., 1987, Choudhari et al., 2006). Hence many researchers are ensuing efforts in order to develop and modify the basicity of MgO for such organic reactions (Menezes et al., 2010, Hattori, 1995, Kantam et al., 2007; Gholinejad et al., 2016; Kantam et al., 2010). The existence of low coordinated acidic and basic sites on surface and corners of MgO have been reported towards active interactions of catalysts with acidic and basic parts of organic molecules (Di Cosimo et al., 2014). It has been successfully demonstrated that low coordinated Mg^{2+} ions at surface and corners act as acidic sites, while low coordinated oxygen anions act as basic site. The 3 coordinated oxygen anions on surface are found to be most reactive (Wu and Goodman, 1992). Generally basic strength of basic sites varies in order $O^{2-}_{3C} > O^{-2}_{4C} > O^{-2}_{5C} > O^{-2}_{6C.}$ (Corma and Iborra, 2006). Thus basic site on the surface of MgO was found responsible for heterolytic cleavage of organic molecules. In this way, surface basicity of MgO plays a key role in proceeding organic reactions. It is also noticed that surface basicity of MgO can be changed by doping other ions in crystal structure of MgO (Zhang et al., 2016). Doping of MgO with metal ions not only changes its electronic properties (Stavale et al., 2012) but also increases number of active basic sites on surface (Ueda et al., 1985). In earlier communications, we have reported that solvent exerts effect on synthesis, particle size and morphology of semiconducting catalysts which, in turn, play very important role in catalytic activity (Kanade et al., 2007, Nakhate et al., 2010). In this context, hydrothermal synthesis is an important technique to obtain unique morphology and desirable particle size (Kanade et al., 2008).

In the present communication, we report the synthesis of pure undoped nanocrystalline and Cu/Fe/Mn doped MgO catalysts. In particular, the effect of particle size, morphology and doping of metal ions on basicity has been investigated in the context of the reported one pot Wittig reaction. The combined effect of doping transition metal in MgO and nanoparticulate nature exerts the synergistic effect on surface basicity enhancement which is evidently beneficial for catalytic application.

2. Experimental

2.1. Chemicals and materials

Commercial MgO, Manganese chloride tetra hydrate ($MnCl_2{\cdot}4H_2O$), Copper chloride dihydrate ($CuCl_2{\cdot}2H_2O$), Ferrous sulphate heptahydrate ($FeSO_4{\cdot}7H_2O$), organic solvents, NaOH flakes, benzaldehyde, ethyl bromoacetate triphenylphosphine are purchased from Loba Chemicals and used without further purification.

2.2. Methods

2.2.1. Preparation of nanocrystalline MgO catalyst

5 g commercial MgO powder was added with stirring to 100 mL 10 M NaOH in 200 mL capacity teflon reactor with stainless still outer jacket. It was then subjected to alkali leached hydrothermal reaction at 180 °C for 24 h. After cooling, the resulting $Mg(OH)_2$ was transferred to 500 mL water in a beaker. It was further diluted and washed with 20 L deionised water and excess alkali was neutralized with very dilute HCl. This content is filtered with suction pump using whatmann filter paper no 41 and dried at 60 °C for 6 h. The magnesium hydroxide obtained by this treatment, was calcined at 450 °C to obtain the nanocrystalline MgO catalyst (Ding et al., 2001).

2.2.2. Preparation of nanocrystalline 1 wt% Cu, Fe, Mn doped MgO catalysts

For the preparation of 1 wt% Cu, Mn and Fe doped nanocrystalline MgO, the desired stoichiometric quantity of each copper chloride dihydrate, manganese chloride tetra hydrate and ferrous sulphate heptahydrate was taken respectively and ground with 5 g commercial MgO for 1 h in a mortar with pestle and each Cu, and Fe and Mn doped crushed MgO samples were subjected to alkali leached hydrothermal method at 180 °C for 24 h. After alkali treatment, the resulting Cu, Fe and Mn doped $Mg(OH)_2$ was transferred to 500 mL water in a beaker. It was further diluted and washed with 20 L deionised water and excess alkali was neutralized with very dilute HCl. This content is filtered with suction pump using whatmann filter paper no 41 and dried at 60 °C for 6 h. The Cu, Fe and Mn doped magnesium hydroxide obtained by this treatment, was calcined at 450 °C to obtain 1 wt% Cu, Fe and Mn doped nanocrystalline MgO catalyst.

The undoped and metal ion doped MgO catalysts were characterized by X-Ray Diffraction (XRD), Field Emission Scanning Electron Microscopy (FESEM), UV-Diffused Reflectance Spectroscopic absorption (UV-DRS), Fourier Transform Infra-Red Spectroscopy (FT-IR), Energy Dispersive X-ray elemental analysis (EDS) and X-ray Photoelectron Spectroscopic (XPS) analysis techniques. XRD analysis of the synthesized material was carried out using Bruker AXS model D-8, (10 to 90° range, scan rate = 1° min^{-1}) equipped with a monochromatic and Ni-filtered Cu Kα radiation. SEM analysis was performed to determine particle morphology of the desired powder catalysts using HITACHI S-4800 model. The UV-DRS spectra were recorded using Shimadzu UV-3600 instrument while the elemental compositional analysis of all MgO catalysts was determined using EDS technique on Bruker XFlash 6130 instrument.

2.2.3. Measurement of catalytic activity for one pot Wittig reaction

(4.7 mmol) benzaldehyde, (4.7 mmol) triphenylphosphine and (4.7 mmol) ethyl bromoacetate were stirred in 5 mL DMF with each catalyst in 25 mL small round bottom flask under ambient conditions. The completions of reactions were monitored by TLC technique using 80% hexane: ethyl acetate mobile phase. After completion of reaction, DMF solvent was added in the reaction mixture and the catalyst was separated by centrifugal separation at 5000 rpm. The separated catalysts were washed with DMF and ethyl acetate and again heated for the next cycle. Reaction mixture was subjected to work up with water and ethyl acetate to remove excess of DMF. The products olefin and triphenylphosphine oxide were purified and separated on silica loaded column using pure hexane as eluent.

The product of Wittig reaction was characterized by High Resolution-Mass Spectra (HR-MS), ^{1}H NMR and ^{13}C NMR technique. For characterization of Wittig reaction product ethyl cinnamate, HR-MS was taken on Bruker Compass Data Analysis 4.2. ^{1}H NMR analysis of products was carried out using Bruker model.

3. Results and discussion

Synthesis of undoped nanocrystalline MgO and Cu/Fe/Mn doped has been carried out using alkali leached hydrothermal method as stated in experimental section. As-synthesized product materials were characterized by using XRD, UV-DRS, FT-IR, FESEM, EDS and XPS analysis.

3.1. X-Ray diffraction analysis

3.1.1. XRD analysis of commercial MgO, Mg(OH)$_2$ and nanocrystalline MgO

Fig. 1 shows the XRD patterns of commercial MgO, magnesium hydroxide and nanocrystalline MgO. The XRD pattern of commercial MgO **(**Fig. 1**a)** shows impurity peaks of Mg(OH)$_2$ at 2θ values 18.50, 37.94, 58.55, while remaining peaks reveal the cubic phase of MgO (JCPDS file no. 44-1482). XRD pattern in **(1b)** demonstrates that XRD peaks mostly match with Mg(OH)$_2$ as evidenced by 2θ values at 18.52, 32.89, 37.99, 50.86, 58.63, 62.05, 68.32 and 72.04°which respectively correspond to 001, 100, 101, 102, 110, 111, 103, 201 planes of hexagonal crystal system of Mg(OH)$_2$ brucite phase (JCPDS file no. 44-1482). The conversion of cubic MgO to hexagonal nanocrystalline Mg(OH)$_2$ can occur due to the leaching effect of highly concentrated alkali in hydrothermal synthesis. However, we intended to synthesize pure nanocrystalline MgO and hence, the as-synthesized Mg(OH)$_2$ was further calcined at 450 °C. At 450 °C, the hexagonal Mg(OH)$_2$ gets completely converted to cubic MgO **(**Fig. 1**c).** The observed 2θ values of XRD pattern (Fig. 1**c)** at 36.91, 42.88, 62.29, 74.68, and 78.61°corresponding to planes 111, 200, 220, 311, 222 matched well with cubic phase of MgO (JCPDS file no. 45-0946). Highly pure nanocrystalline cubic phase of MgO synthesized in this way has been subsequently used for transition metal doping and catalytic study.

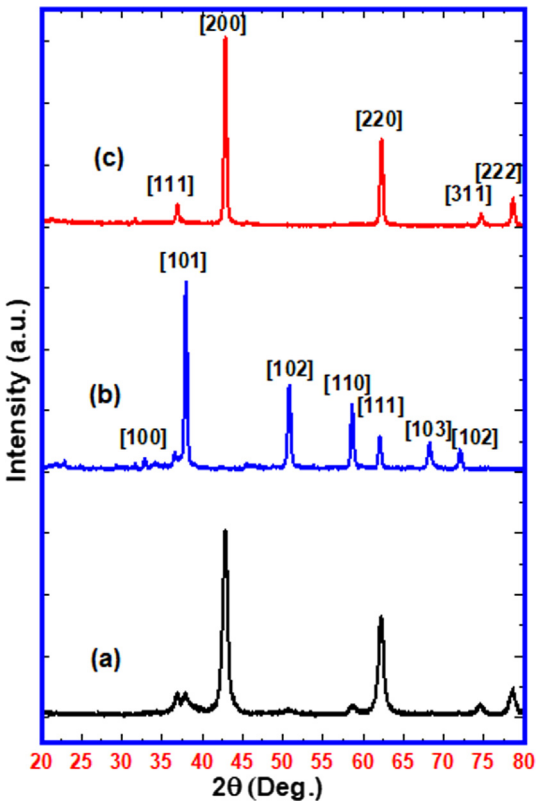

Fig. 1 XRD patterns of (a) Commercial MgO (b) Mg(OH)$_2$ (c) Synthesized nanocrystalline MgO.

3.1.2. Effect of calcination temperature on crystallite size of nanocrystalline MgO

Fig. 2 displays the X-ray diffraction patterns of nanocrystalline MgO calcined under different temperatures viz. 450 °C, 700 °C and 900 °C. For surface activation of MgO and for tuning of crystallite size, calcination at suitable temperature is recommended (Lee et al., 2009). The average crystallite sizes for nanocrystalline MgO particles were calculated for different calcination temperatures by using Scherer's equation at [200] plane. Under no activation (i.e no heating) condition, although the commercial MgO disclosed smallest crystallite size, it indicated presence of surface hydroxide impurity. On raising the calcination temperature from 450 °C to 700 °C, the crystallite size appears to be reduced from 26 nm to 17 nm. Apparently, we observed the smallest crystallite size for the sample calcined at 700 °C for 4 h calcination time. On increasing the calcination temperature up to 900 °C, crystallite size appears to increase again. The observed irregularity in crystallite size variation as a function of calcination temperature may be attributed to changing crystallinity pattern and intrinsic defects (Zhang et al., 2015a,b). Thus, the calcination temperature 700 °C was found to be optimum for surface activation as it yields smallest crystallite size.

3.1.3. XRD analysis of 1 wt% Cu/Fe/Mn doped MgO

Fig. 3 shows the XRD patterns corresponding to pure (undoped) nanocrystalline MgO, 1 wt% Cu doped MgO**,** 1 wt%

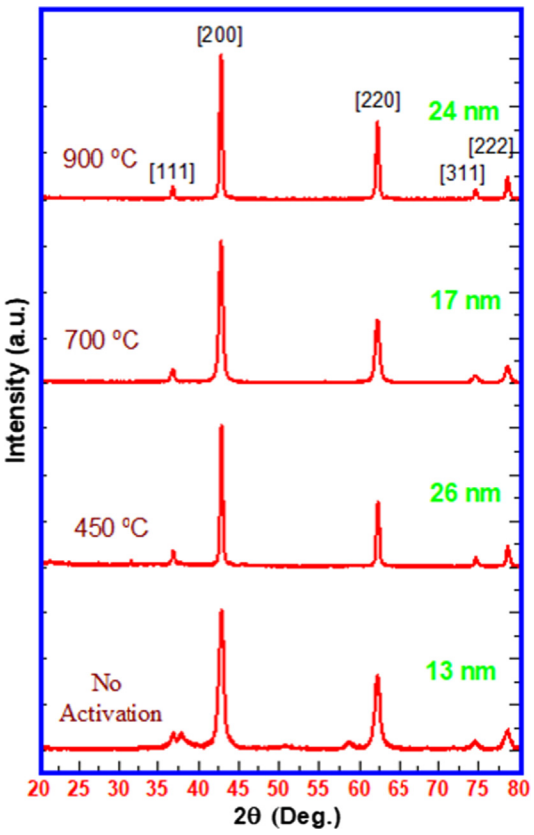

Fig. 2 Effect of calcination temperature on crystallite size of nanocrystalline MgO.

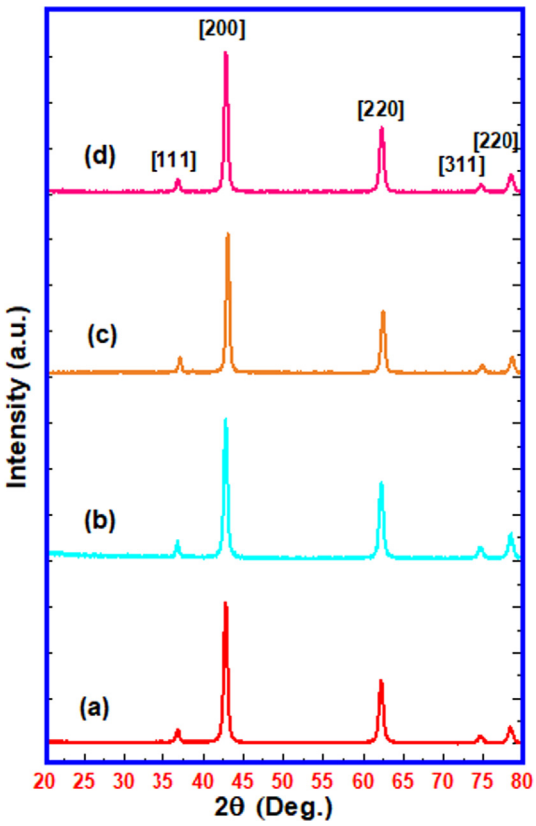

Fig. 3 XRD patterns of (a) Nanocrystalline MgO, (b) 1 wt% Cu doped MgO (c) 1 wt% Fe doped MgO and (d) 1 wt% Mn doped MgO catalysts calcined at 700 °C.

Fe doped MgO and 1 wt% Mn doped MgO. All XRD peaks are in agreement with JCPDS values for cubic phase of MgO (JCPDS file no. 45-0946). The effect of doping by Cu, Fe and Mn in nanocrystalline MgO has not been predominantly observed as expected in terms of shifting of the peaks. The average crystallite size calculated by using Scherer's equation at [200] plane is observed in the range of 16–19 nm. The undoped nanocrystalline MgO and 1 wt% Fe doped nanocrystalline MgO catalysts show the crystallite size of 17 nm. 1 wt% Cu doping in nanocrystalline MgO leads to crystallite size of 19 nm for the resultant catalyst sample while 1 wt% Mn doping in nanocrystalline MgO leads to smallest crystallite size of 16 nm for the resultant catalyst sample. For the measurement of the catalytic efficiency, 1 wt% Cu, Fe and Mn doped nanocrystalline MgO samples were used.

3.2. UV-diffused reflectance analysis

Fig. 4 displays the UV diffused reflectance spectra of undoped and 1 wt% Cu/Fe/Mn doped MgO nanomaterials. Undoped nanocrystalline MgO reveals formation of pure phase (Fig. 4**a**) with absorption band around 274 nm. In case of 1 wt% Fe doped MgO sample, absorption band exhibits red shift at 347 nm (Fig. 4**b**). In case of 1 wt% Cu doped MgO sample, two sharp absorption bands at 230 nm and 274 nm are observed along with red-shifted band at 552 nm (Fig. 4**c**). Similarly, for 1 wt% Mn doped MgO sample, two absorption bands (located at 228 nm and 281 nm) as well as one red-shifted band (located at 482 nm) have been noticed

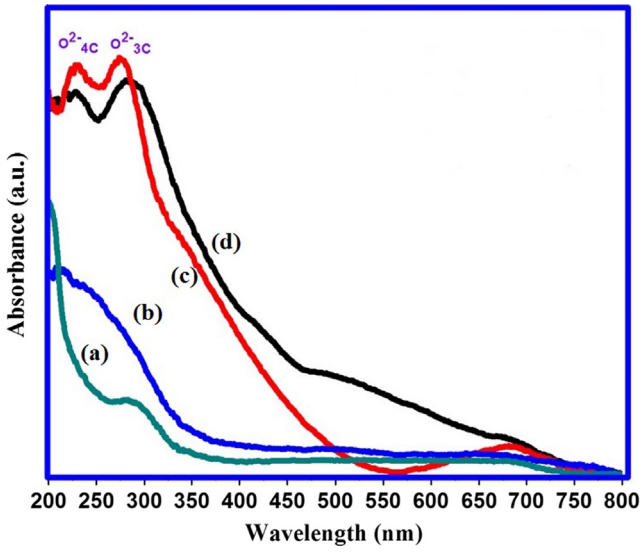

Fig. 4 UV-DRS spectra of (a) undoped nanocrystalline MgO (b) 1 wt% Fe doped MgO (c) 1 wt% Cu doped MgO and (d) 1 wt% Mn doped MgO.

(Fig. 4**d**). These multiple sharp absorption bands in UV-DRS spectra form an important tool for gaining an insight into distribution of surface basicity of MgO (Coluccia and Tench, 1979). Fig. 4c and 4d illustrate multiple absorption

bands in UV-DRS of 1 wt% Cu and Mn doped MgO nanocrystalline materials. The absorption bands mainly at 228 and 281 nm may be related to low coordinated oxygen at surface, corners and kinks of MgO system as reported by Zhang et al. (2015).

The strength and number of this low coordinated oxygen is responsible for the enhancement of surface basicity. It is also reported that UV absorption at 280 nm corresponds to excitation of 3 coordinated oxygen atom at surface and UV absorption at 230 nm is associated with excitation of 4 coordinated oxygen (Hattori, 2004).

In our case, similar absorption bands for undoped, Cu doped and Mn doped MgO materials are observed implying presence of low coordinated oxygen yielded in Cu and Mn doped nanomaterials which, in turn, can effectively enhance the catalytic efficiency for the proposed reaction. The Fe doped MgO nanomaterial does not show any absorption band. It indicates the absence of low coordinated oxygen at surface probably due to preferential formation of Fe-O interface bias layer on the surface of FeO as reported earlier (Fan et al., 2013). Overall UV-DRS study shows that the proposed methodology for synthesis of transition metal doped MgO has certain intrinsic advantages, which might be beneficial to increase number of low coordinated oxygen in Cu and Mn doped MgO nanomaterial. Hence, as-synthesized doped MgO nanomaterials were further used as heterogeneous basic catalysts in reported one pot Wittig reaction.

3.3. Fourier transform infra-red analysis

Fig. 5 shows the FT-IR spectra of nanosized undoped and 1 wt % Cu/Fe/Mn doped MgO catalysts. It is fairly established that FT-IR analysis is an important tool to obtain information about nature of surface oxygen in MgO (Hadia and Mohamed, 2015). The similar absorption regions for Mg—O stretching frequencies are observed in the range of 400–850 cm^{-1} (Fig. 5). In the first region, the bands due to different fundamental Mg—O vibrations are observed between 400 and 500 cm^{-1} (Raman, 1961). In the second region, combination bands of fundamental vibrations appeared between 550 and 850 cm^{-1} (Raman, 1947). Two bands appeared between 1400 and 1500 cm^{-1} in all undoped and Cu/Fe/Mn doped nanosized catalysts indicating the adsorption of CO_2 on MgO surface as reported previously (Philippt and Fujimoto, 1992). In case of Fe doped MgO catalyst, these absorption bands are significant which might be due to adsorption of CO_2 and its spongy nature as observed in FESEM photographs. Absence of bands in the region 3400–3600 cm^{-1} specifies the purity of material

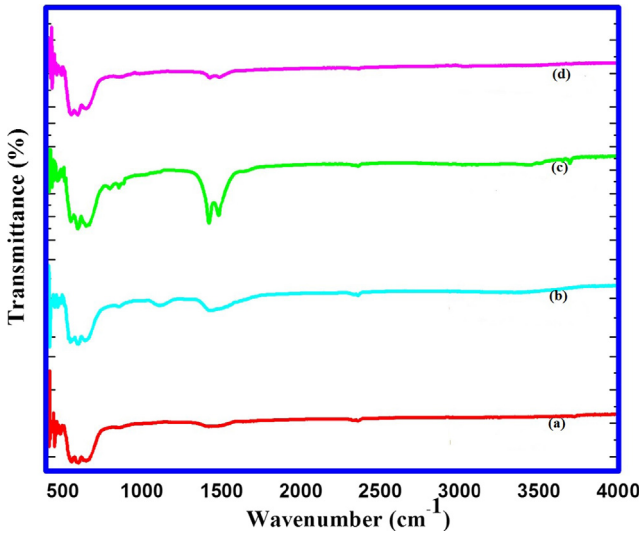

Fig. 5 FT-IR spectra of (a) nanocrystalline MgO (b) 1 wt% Cu doped MgO (c) 1 wt% Fe doped MgO and (d) 1 wt% Mn doped MgO.

3.4. Field emission scanning electron microscopic analysis

Fig. 6 presents FESEM photographs of pure and doped nanocrystalline MgO catalysts which, by and large, disclose formation of hexagonal plates. The average particle size of hexagonal plates of nanocrystalline MgO is 68 nm and thickness appears to be 18 nm (Fig. 6**a–b).** The 1 wt% Fe/MgO catalyst shows spongy/porous hexagonal plates with the average particle size of 240 nm, thickness of 32 nm and average pore size of 10 nm (Fig. 6**c–d).** The hexagonal plates of 1 wt% Cu/MgO show average particle size of 450 nm and thickness of 70 nm **(**Fig. 6**e–f).** The 1 wt% Mn/MgO catalyst displays formation of nanosheets and spherical particles. The thickness of nanosheet is 21 nm while the length and breadth are in the order of micron size. The spherical particles of 1 wt% Mn/MgO catalyst indicate average diameter of 180 nm **(**Fig. 6**g–h).** All these FESEM observations confirm formation of nanomaterials with distinct morphology.

3.5. Energy dispersive X-ray spectroscopy (EDS) for elemental analysis

Fig. 7 furnishes typical EDS elemental analysis data for 1 wt% Cu, 1 wt% Fe and 1 wt% Mn doped MgO catalysts. The recorded spectra endorse presence of Cu, Fe and Mn metal in MgO material. In case of Cu doping in MgO, the normalized weight % for Cu is found to be 1.02**%** **(**Fig. 7**a)** while for Fe doped MgO, the normalized weight % for Fe is found to be 0.73% **(**Fig. 7**b)** and in case of Mn doped MgO, the normalized % weight for Mn is found to be 1.34% **(**Fig. 7**c)**. The pertinent EDS data evinces that doping of transition metals in nanocrystalline MgO matrix takes place successfully.

3.6. XPS analysis

X-ray photoelectron spectroscopic analysis was performed for identification of oxidation state of catalyst elements and to determine the strength of basic catalysts. Fig. 8 furnishes the XPS scans displaying binding energy (BE) peaks (deconvulated) for Mg 2P and O 1S energy states in pure nanocrystalline MgO and 1 wt% Cu, Fe and Mn doped MgO. After carbon correction, binding energy values for Mg 2P energy states are observed at 49.8, 49.6, 49.4 and 48.8 eV respectively. In case of XPS peak of O1S energy state, each peak is deconvulated into three peaks. The smallest value peak represents lattice oxygen, middle value peak represents surface hydroxides and largest value peak represents the surface carbonates. Accordingly, lattice oxygen XPS peaks for pure, Cu, Fe and Mn doped MgO catalysts are observed at 529.6, 529.3, 528.92 and 529.6 eV respectively (Fig. 8a-8d). In XPS analysis,

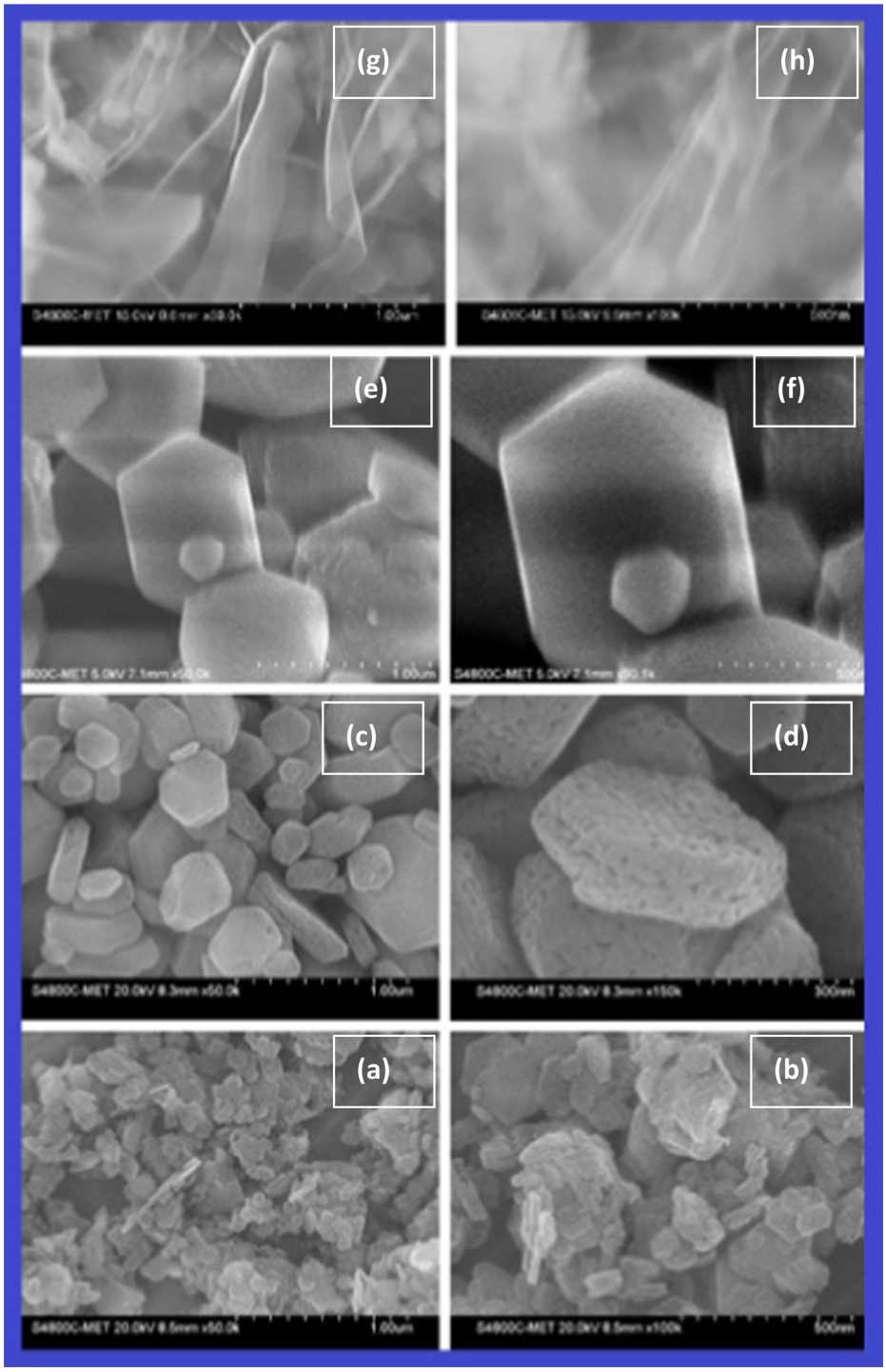

Fig. 6 FESEM images of (a-b) Nanocrystalline Pure MgO, (c-d) 1 wt% Fe doped MgO, (e-f) 1 wt% Cu doped MgO, (g-h) 1 wt% Mn doped MgO.

binding energy of $2P_{3/2}$ energy state is very important diagnostic peak for distinguishing different oxidation states of transition metals. Fig. 9 provides XPS scans showing BE peaks for $2P_{3/2}$ and $2P_{1/2}$ energy states of Cu, Fe and Mn elements in doped MgO catalysts (Fig. 9a-9c). It may be recalled that all pure undoped and doped nanocrystalline MgO catalysts are calcined at 700 ^{O}C. In the context of XPS analysis in Fig. 9, for Fe doped MgO catalyst, the XPS peak at 709.4 might be ascribed to presence of Fe (II) in MgO (Fig. 9a). The binding energy peaks of $2P_{3/2}$ energy states appeared at 932.7 eV might be ascribed to presence of Cu (II) which is strongly distinguished from Cu (I) and Cu(0) by presence of strong Cu (II) satellite peak at 940.4 eV (Fig. 9b). The presence of XPS peak at 641.8 eV is ascribed for Mn (IV) in MgO catalyst (Fig. 9c). Doublet at this position confirms the absence of other oxidation state of Mn in MgO (Vasquez, 1998; Mansour and

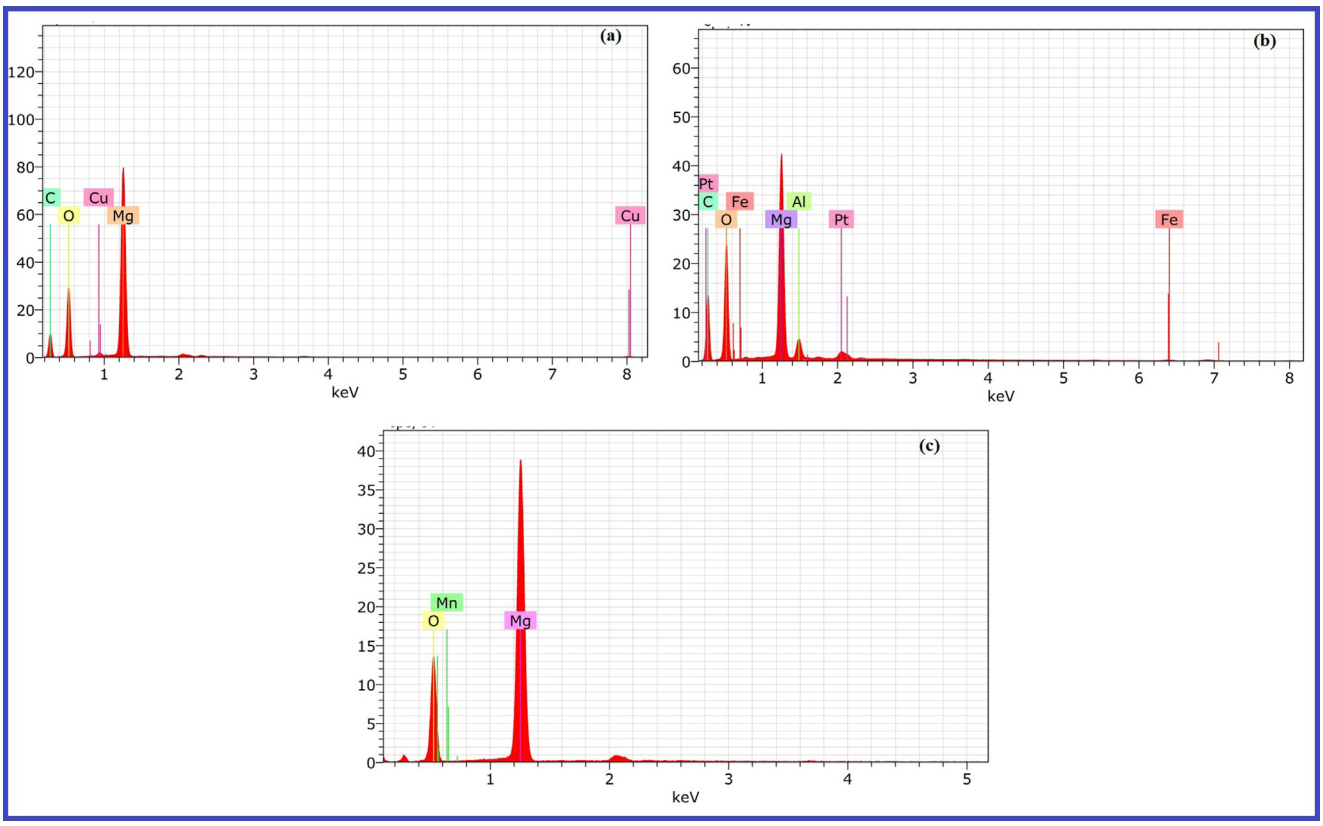

Fig. 7 EDS Elemental Analysis of (a) 1 wt% Cu doped MgO, (b) 1 wt% Fe doped MgO and (c) 1 wt% Mn doped MgO.

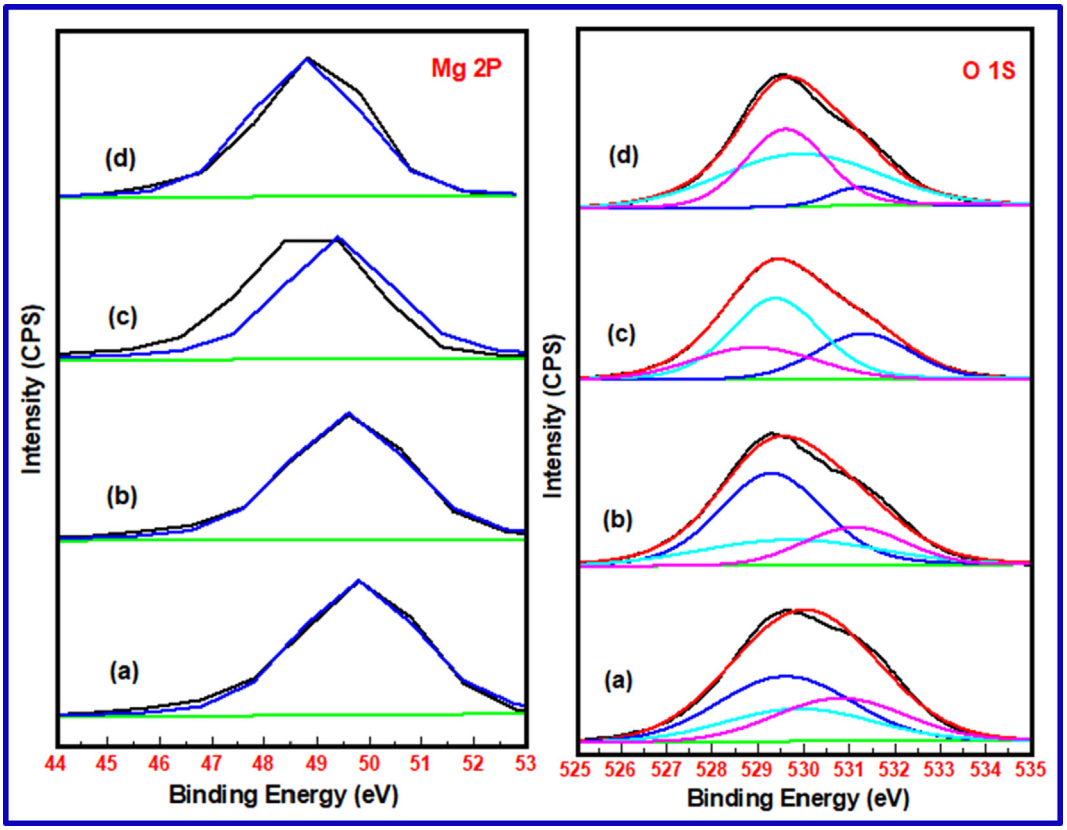

Fig. 8 XPS Scans of Mg 2P and O 1S energy states in a) pure nanocrystalline MgO b) 1 wt% Cu doped MgO c) 1 wt% Fe doped MgO d) 1 wt% Mn doped MgO.

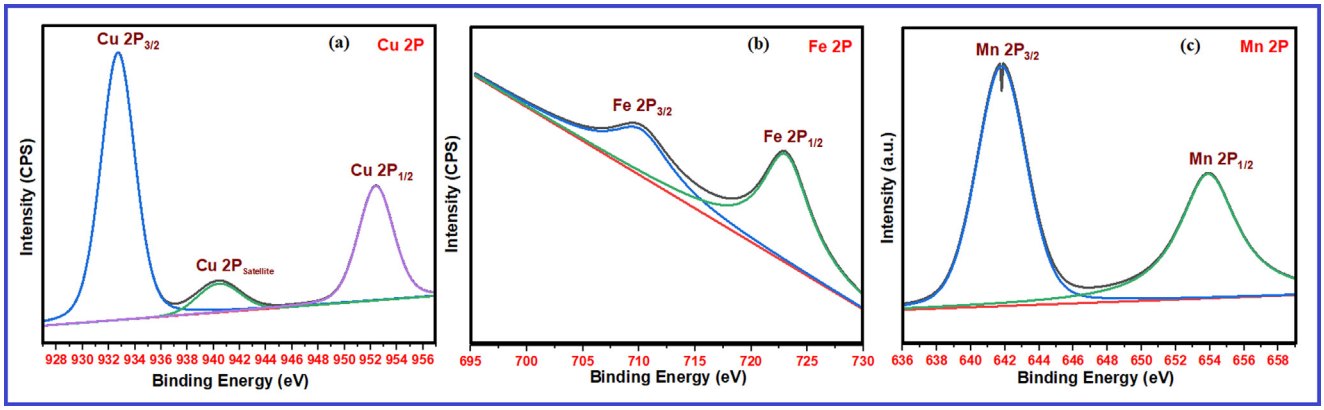

Fig. 9 XPS scans corresponding to 2P energy states in a) 1 wt% Cu doped MgO b) 1 wt% Fe doped MgO c) 1 wt% Mn doped MgO.

Brizzolara, 1996; Nesbitt and Banergee, 1998; Stranick, 1999). It is worthwhile to note that at higher calcination temperature under oxidising condition, Mn exists in higher oxidation state in MgO.

High resolution XPS scans corresponding to Mg 2p and O 1s energy states of pure and doped MgO catalysts elucidate that doping of Cu, Fe and Mn elements in MgO can cause shifts in pertinent binding energy values presumably due to change in surface basicity. On the contrary, surface basicity of MgO like solid bases can be correlated with binding energy of O 1S energy states (Vedrine, 2015).

As a general rule, low binding energy values of O 1S energy state increases the surface basicity and vice versa (Hattori, 1995). Qualitatively, it is very difficult to predict the surface basicity of surface oxygen just by looking at increase or decrease of binding energy values of O 1S energy states, rather relative binding energy difference (**ΔB.E)** between O 1S and Mg 2P energy states and binding energy shifts (Moulavi et al., 2019) are useful for comparative evaluation of surface basicity values of the same basic catalysts. Table 1 illustrates the relative binding energy difference between O 1S and Mg 2P energy states and binding energy shift for pure and Cu, Fe and Mn doped MgO basic catalysts calcined at 700 °C.

From shifts in binding energy values as stated in Table 1, it is seen that binding energy of 1 wt% Cu doped MgO basic catalyst is increased by only 0.1 eV while for 1 wt% Fe doped MgO it is increased by 0.28 eV. Interestingly, 1 wt% Mn doping in MgO shows drastic decrease in binding energy by 1.0 eV. From such observations, it is argued that doping of 1 wt% Mn in MgO leads to enhancement of surface basicity of MgO catalyst compared to that of 1 wt% Cu and Fe doped MgO catalysts. As doping of Cu and Fe is responsible for increasing the binding energy of MgO system, this increased and decreased charge of Mg and O must be compensated by transition metal dopant in MgO crystallites. These elements after doping exist in oxide forms. Hence, this charge compensation can be calculated by considering again relative binding energy difference of transition metal ions $2P_{3/2}$ and O 1S energy states and binding energy shifts between standard CuO, FeO and MnO_2 with that of observed for the same doped elements in MgO. Table 2 shows the relative binding energy difference of $2P_{3/2}$ and O 1S energy states and binding energy shift for standard corresponding oxides with that of the observed ones.

From Table 2, it is reflected that although binding energy of MgO in 1 wt% Cu and Fe doped MgO increases, this charge is not compensated by dopant Cu and Fe in MgO matrix, while binding energy of MgO in 1 wt% Mn doped MgO decreases. This increased charge of Mg and decreased charge of O elements are compensated by Mn under oxidising environment. Due to higher variable oxidation state of Mn in MgO, decrease in binding energy of MgO is significant and this charge is considerably compensated. From the XPS analysis, it is confirmed that higher oxidation state Mn (IV) is responsible for enhancement of surface basicity of MgO basic catalyst by the virtue of surface electron donor characteristic attributed to variable oxidation state.

3.7. Measurement of catalytic activity

In the present work, we report an efficient one-pot, three component Wittig reaction for the synthesis of ethyl cinnmate in the presence of nanocrystaline MgO (undoped and Cu, Fe, Mn doped) as highly effective heterogeneous base catalysts at room temperature **(**Scheme 1**).** This protocol involves syner-

Table 1 Relative binding energy difference and binding energy shift between O 1S and Mg 2P energy levels in 1 wt% Cu, Fe and Mn doped nanocrystalline MgO.

No	Catalysts	Binding energy eV			Shift in B. E.
		O1S	Mg2P	ΔB.E	
1	Nanocrystalline MgO	529.6	49.8	479.8	0.0
2	1 wt% Cu/MgO	529.3	49.6	479.7	+0.1
3	1 wt% Fe/MgO	528.92	49.4	479.52	+0.28
4	1 wt% Mn/MgO	529.6	48.8	480.8	−1.0

Table 2 Relative binding energy difference between $2P_{3/2}$ and O 1S energy levels and binding energy shift in standard corresponding oxides with reference to observed ones.

No.	Samples	Binding energies of oxides eV				Binding energy difference eV		B. E. Shift
		Standard		Observed		Standard	Observed	
	Energy states	$2P_{3/2}$	O 1S	$2P_{3/2}$	O 1S	$2P_{3/2}$	O 1S	
1	1 wt% Cu/MgO	933.45	529.40	932.7	529.3	404.05	403.4	+0.65
2	1 wt% Fe/MgO	710.1	529.60	709.4	528.92	180.5	180.48	+0.02
3	1 wt% Mn/MgO	642.4	529.60	641.8	529.6	112.8	112.2	+0.6

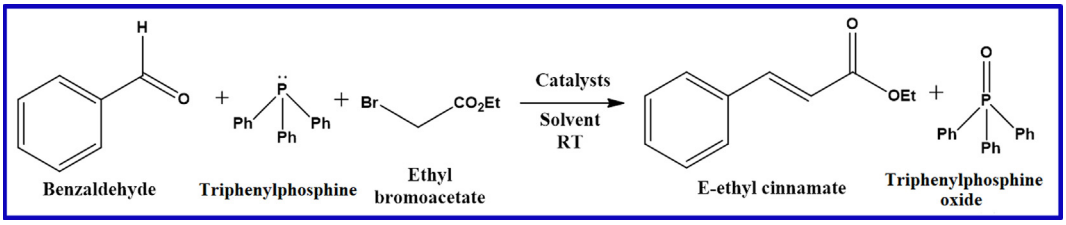

Scheme1 One pot Wittig reaction of benzaldehyde, triphenylphosphine, ethyl bromoacetate in presence of MgO catalysts.

gistic effect of doping transition metals in crystal structure of MgO and nanocrystalline size in enhancing the surface basicity of MgO for one pot Wittig reaction.

3.7.1. Effect of calcination temperature on activation of catalyst

To optimize the activation temperature of catalysts, the Wittig reaction (Scheme 1) was performed using undoped nanocrystalline MgO heated at different activation temperatures. The undoped catalysts are heated at temperature 120, 450, 600, 700 and 900 °C and used further as catalyst. In our present study, we found that nanocrystalline MgO heated at 700 °C exhibits maximum catalytic efficiency (Fig. 10). The activity is less below the temperature 700 °C because active basic sites of MgO surface could have been possibly masked by adsorption of CO_2 and water vapors at lower temperatures. Accordingly, gradual increase of catalytic activity with increase in temperature is due to removal of CO_2 and water vapors from surface resulting into activation of MgO surface basic sites (Tanabe and Yamaguch, 1964). It is also observed that activation temperature of catalyst is different for different reactions (Gadge et al., 2014). Thermal activation of pure nanocrystalline MgO at 700 °C exhibits smallest crystallite size as observed by XRD study. Whereas at temperatures above 700 °C, catalytic activity decreases which may be attributable to increase in particle size and impurity influenced crystalline behavior (Zhang et al., 2015). Therefore, for further study, all doped and undoped catalysts are activated at 700 °C prior to use in one pot Wittig reaction.

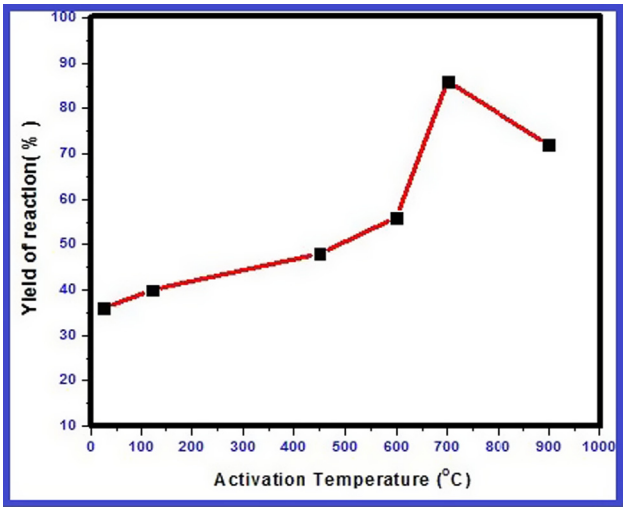

Fig. 10 Effect of temperature on activation of nanocrystalline MgO.

3.7.2. Effect of solvent

Catalytic efficiency of activated nanocrystalline MgO is obtained for different solvents in one pot Wittig reaction. It is observed that nanocrystalline MgO catalyst has maximum catalytic efficiency in polar aprotic solvent DMF with 81% yield at room temperature, whereas, only 40% yield has been obtained for toluene as solvent under the same reaction conditions (Table 3). Mechanism of reaction is well understood. During reaction, intermediates such as phosphonium salt, phosphorus ylide, betaine and oxa-phosphetane are formed. The polarity of solvent may play role in formation and stabilization of these intermediates. For this reason, more yield is observed with polar solvent while minimum yield is observed for non-polar solvent.

3.7.3. Effect of doping of Cu, Fe and Mn on catalytic activity of MgO

Specific amount (200 mg) of activated catalyst was used for one pot Wittig reaction in DMF solvent. The end product ethyl cinnamate was characterized by TLC, HR-MS, ^{1}H NMR and ^{13}C NMR spectroscopic techniques. 1 wt% Mn doped MgO nanocatalyst shows better catalytic activity with 86% yield (Table 4, **entry 6**). Whereas only 56% yield is

Table 3 Effect of solvent on catalytic activity of Nanocrystalline MgO in one pot Wittig reaction.

Solvent	DMF	Acetonitrile	THF	Ethyl alcohol	Toluene	DMSO
% yield[a]	81	61	45	57	40	72

Reaction condition: 4.7 mmol benzaldehyde, 4.7 mmol TPP and 4.7 mmol ethyl bromo acetate are stirred with 200 mg nano MgO in each 5 mL solvent at RT.
[a] Isolated yield.

Table 4 Effect of Cu, Fe and metal ion doping on catalytic activity of MgO.

No	Catalysts	Reaction time/Hr	Yield[a]/%	Particle size Thickness (Length)	Morphology	E/Z ratio[b]
1	Blank reaction	24	0	–	–	–
2	Commerical MgO	12	60	1–2 μm	Irregular	99:1
3	Nanocrystalline MgO	12	81	18(68) nm	Hexagonal plates	95:5
4	1% Fe/MgO	12	56	32(240)nm	Hexagonal plates	99:1
5	1% Cu/MgO	12	70	70(450) nm	Hexagonal plates	96:4
6	1% Mn/MgO	12	86	21(> 1000) nm	Nanosheets	95:5

Reaction conditions: benzaldehyde (4.7 mmol), TPP (4.7 mmol) and ethyl bromo acetate (4.7 mmol) are stirred in 5 mL DMF with each catalysts at RT for 12 h stirring.
[a] Isolated yield.
[b] Entgegen/Zusammen ratio is calculated from integration lines in ^{1}H NMR spectra of crude products after column chromatography.

obtained for Fe doped MgO catalyst. Doping of Fe in MgO decreases the number and strength of basic sites (Table 4, **entries 4)**. Undoped nanocrystalline MgO catalyst has 81% yield (Table 4, **entry 3)**. It is more than that of commercial MgO and may be attributed to relative increase in the surface area and prismatic, hexagonal morphology of nanocrystalline MgO as observed in FE-SEM analysis. However, increase in particles size of Mn doped nanocrystalline MgO does not affect the yield due to more surface basicity by the virtue of surface donor properties of Mn due to its higher oxidation state (Stavale et al., 2012) as well as more number of low coordinated oxygen as observed in UV -DRS study. Cu doped MgO nanomaterial shows 70% yield (Table 4, **entry 5)** which is lower than pristine nanocrystalline MgO due to decreased basicity, though it has more number of low coordinated oxygen at surface. Decrease in surface basicity of MgO is due to doping of Cu which decreases the strength of basic sites as observed by XPS. (Pudi et al., 2015). One more reason for decrease in the catalytic activity of Cu doped MgO materials is incorporation of Cu metal in MgO lattice at high temperature heating required for activation (Zhang et al., 2016). However, lower yield obtained for Fe doped MgO (Table 4, **entry 3)** may be due to formation of exchange bias layer of FeO on surface which decreases the number of low coordinated oxygen on surface and corners as expected due to heating at high temperature (Fan et al., 2013). Besides, doping of Fe in MgO increases the acidity due to small size of Fe (Ueda et al., 1985). The blank reaction is subjected to proceed without use of any catalyst. It shows no formation of olefin and triphenyl phosphonium oxide on TLC and isolated yield is 0% (Table 4, **entry 1)** confirming the reaction is really a base catalysed.

Thus, proposed Wittig reaction revealed maximum yield for 1 wt% Mn doped nanocrystalline MgO. Further optimization of amount of precursors used in the Wittig reaction was carried out by keeping the same amount of catalyst and by varying the concentrations of the precursors under the same reaction conditions. After optimizing the precursors, amount of catalysts was also optimized using the optimized concentration of the precursors under the same reaction conditions.

Characterization of Wittig product

(1) Table 4, Entry 2 (Commercial MgO)

HR-MS: [M + H] = 177.09 (calculated for $C_{11}H_{12}O_2$ – 176.21),

^{1}H NMR: (400 MHz, $CDCl_3$): 1.34 ppm triplet 3H (J = 7.6 Hz), 4.26 ppm quartet 2H (J = 7.2 Hz), 6.43 ppm doublet 1H (J = 16 Hz), 7.38 ppm triplet 3H, 7.52 ppm 2H, 7.68 ppm doublet 1H (J = 16 Hz).

(2) Table 4 Entry 3 (Nanocrystalline MgO)

^{1}H NMR: (500 MHz, $CDCl_3$)1.34 ppm triplet 3H (J = 5 Hz), 4.25 ppm Quartet 2H J = 5 Hz, 6.41 ppm doublet 1H J = 20 Hz, 7.25–7.52 ppm 5H multiplet. 7.66 δ Doublet J = 20 Hz 1H,

^{13}C NMR: (500 MHz, $CDCl_3$) 14.38 δ, 60.35 δ, 118.31 δ, 128.02, 120.04 δ, 129.75 δ, 130.14 δ, 144.54.

(3) Table 4 Entry 4 (1 wt% Fe/MgO)

^{1}H NMR: (400 MHz, $CDCl_3$)1.34 ppm triplet 3H (J = 8 Hz), 4.25 ppm Quartet 2H J = 7.0 Hz, 6.43 ppm doublet 1H J = 16 Hz, 7.37–7.54 ppm 5H multiplet. 7.68 δ Doublet 1H J = 16 Hz,

(4) Table 4 Entry 5 (1 wt% Cu/MgO)

Table 5 Effect of concentration of reactants and catalyst amount on catalytic activity of 1% Mn doped MgO.

No	Reactants stichoimetry/No of equivalents			Catalyst Amount/Mg	Reaction Time/h	Yield[a] %
	Benzaldehyde	TPP	Ethyl bromoacetate			
1	1	1	1	200	12	86
2	1	1.2	1.2	200	10	85
3	1.2	1	1	200	9	92
4	1.5	1	1	200	8	94
5	1.5	1	1	100	7	98
6	1.5	1	1	50	10	70

Reaction conditions: 1% Mn doped MgO activated catalyst is stirred with reactants in 5 mL DMF solvent at RT.
[a] Isolated yield.

^{1}H NMR: (500 MHz, $CDCl_3$) 1.33 ppm triplet 3H (J = 7.5 Hz), 4.27 ppm Quartet 2H J = 7.2 Hz, 6.44 ppm doublet 1H J = 16 Hz, 7.32–7.53 ppm 5H multiplet., 7.68 δ Doublet 1H J = 16 Hz,

(5) Table 4 Entry 6 (1 wt% Mn/MgO)

^{1}H NMR: (500 MHz, $CDCl_3$) 1.32 ppm triplet 3H (J = 7.5 Hz), 4.25 ppm Quartet 2H J = 7.0 Hz, 6.42 ppm doublet 1H J = 16 Hz, 7.31–7.58 ppm 5H multiplet, 7.68 δ Doublet 1H J = 16 Hz,

3.7.4. Effect of concentration of precursors and catalysts amount on catalytic activity of Mn doped MgO

Table 5 shows the effect of varying concentrations of benzaldehyde, triphenylphosphine, ethyl bromoacetate and catalysts amount on the catalytic activity of 1 wt% Mn doped MgO. On increasing the concentration of triphenylphosphine and ethyl bromo acetate from 1 to 1.2 equivalents, it shows negligible effect on rate and catalytic efficiency of the reaction **(**Table 5**, entry 2)**. But on increasing the concentration of benzaldehyde from 1 to 1.5 equivalent, it affects the rate and catalytic efficiency drastically **(**Table 5**, entry 3, 4)**. Under this optimized concentration of the reactants, catalyst amounts are varied from 200 mg to 50 mg. Best results are obtained in presence of 100 mg catalyst when we stirred 1.5 equivalent benzaldehyde with 1 equivalent of TPP and 1 equivalent of Ethyl bromo acetate **(**Table 5**, entry 5)**.

We speculate that 1 wt% Mn doped nanocrystalline MgO is an eco-friendly and efficient catalyst for one pot Wittig reaction between 1.5 equivalent of benzaldehyde and 1 equivalent of triphenylphosphine with 1 equivalent of ethyl bromoacetate.

As shown in Table 5, entry 5 the presently reported 1 wt% Mn doped nanocrystalline MgO catalyst has 98% yield for 1.5:1:1 of benzaldehyde, triphenylphosphine and ethyl bromoacetate precursors, respectively for 100 mg catalyst amount in DMF solvent at room temperature. The yield reported in this investigation is higher than that reported by Choudhari et al. (2006) for nanocrystalline MgO. We also report that the catalyst ratio used in our approach is almost less than half than the earlier reported value.

3.7.5. Mechanistic study

The mechanism of Wittig reaction is well known under homogeneous condition. However, it is very interesting to see its mechanism on surface of catalysts under heterogeneous condition. Catalyst performs very important role firstly in providing acidic and basic sites for interaction with organic molecules for the formation of polar phosphonium salts, secondly deprotonation of phosphonium salts to form phosphorus ylides,

To confirm the above outcomes of mechanistic details, the intermediate phosphonium bromide salt was stirred with benzaldehyde in presence of catalyst **(**Scheme 2**).**

When 4.7 mmol of phosphonium salt was stirred with 4.7 mmols benzaldehyde in absence of catalyst, even after 15 h, only 3% conversion of olefin was obtained **(**Table 6**, entry 1)**.

It means that deprotonation of phosphonium salt is slow and hence the rate determining step of the reaction. After adjusting benzaldehyde stichoimetry from 1 to 1.5 equivalent, reaction proceeds with quantitative yield of 98% within short period of time (Table 6**, entry 4, 5**). Based on these experiments, mechanism of on pot Wittig reaction is proposed on surface of catalyst **(**Scheme 3**).** In reactions, different types of charged intermediates are formed such as betaine, oxaphosphetane etc. after nucleophilic addition of polar phosphorane to benzaldehyde. Surface of catalysts is responsible for stabilization and formation of these intermediates. Finally oxaphosphetane intermediate collapses into products. Catalysts and products are separated by centrifugation and catalyst is activated for the next cycle of reaction.

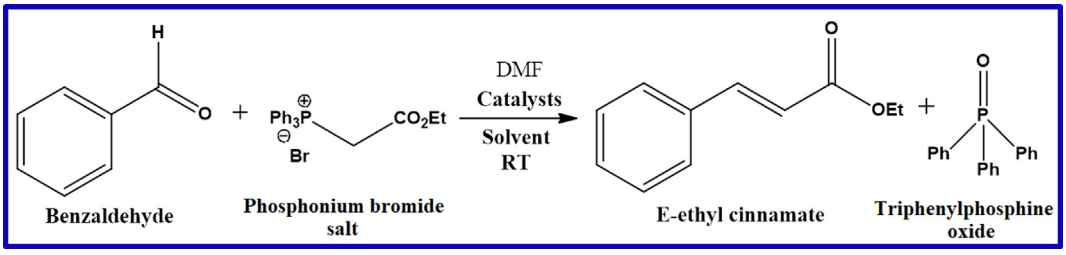

Scheme 2 Reaction of intermediate phosphonium bromide salt with Benzaldehyde.

Table 6 Mechanistic investigation of one pot Wittig reaction by reaction with intermediate phosphonium salt.

No	Reactants stoichiometry		Catalysts	Reaction Time/h.	Yield/%
	Benzaldehyde	Phosphonium salt			
1	1	1	–	15	3
2	1	1	100 mg	10	95
3	1.2	1	100 mg	8	96
4	1.5	1	100 mg	6	98

Reaction condition: Phosphonium salt is stirred with benzaldehyde in presence of 100 mg catalysts in 5 mL DMF solvent at RT.

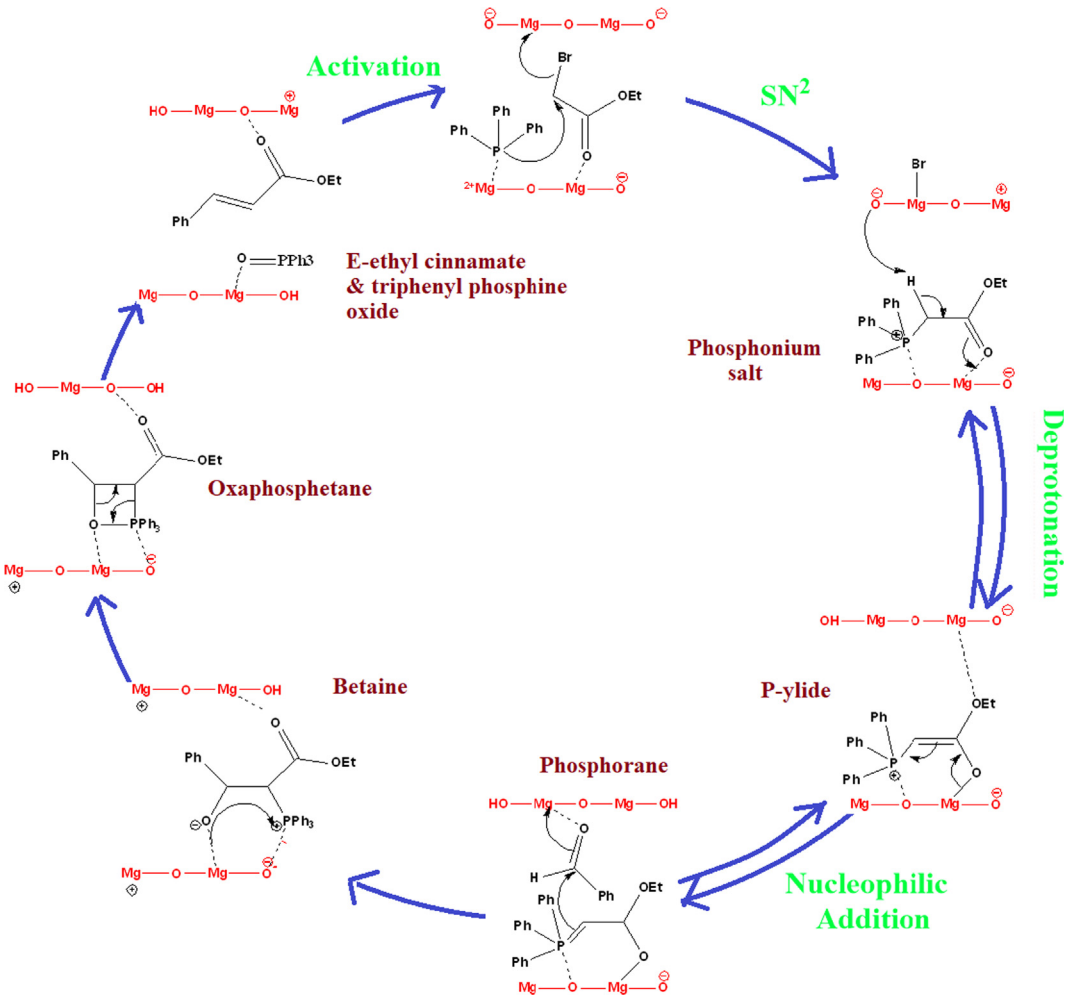

Scheme 3 Proposed mechanism of one pot Wittig reaction on surface of MgO catalyst.

Thus, we have enhanced the basicity of nanocrystalline MgO catalyst by doping transition metal Mn for the effective use in the one pot Wittig reaction. Our methodology is eco-friendly and easy to scale up for the different types of Wittig reactions. We also supported the mechanism of reactions by changing the concentration of reaction precursors and studied the same reaction in two steps

3.7.6. Recycling study

Fig. 11 presents the recycling data of nanocrystalline 1 wt% Mn doped MgO catalyst under the optimized reaction conditions. The catalyst is recycled five times without significant loss in the catalytic activity with almost the same recovery. After each cycle, catalyst was separated by simple centrifugation and washed with DMF and ethyl acetate. For each cycle, the separated catalysts again reactivated by heating at 700 °C and reused for the next cycle of Wittig reaction. The phase and purity of 1% Mn doped MgO as catalyst is studied before and after reaction using XRD technique which substantiates that no significant change has been observed in phase and purity of catalyst.

In nutshell, we have demonstrated novel approach to obtain high yield for Wittig reaction compared to other MgO based catalysts. The effect of particle size, morphology

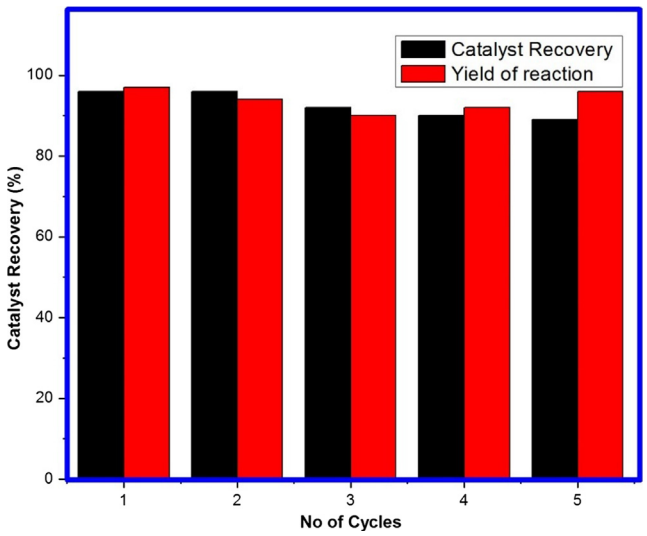

Fig. 11 Recycling of 1 wt% Mn doped MgO catalyst.

and dopant material of catalyst was successfully studied for the reported reactions. Mn doped MgO catalyst was found to be an efficient catalyst to proposed reaction.

4. Conclusions

Nanocrystalline catalytic systems comprising undoped MgO as well as Cu, Fe and Mn doped MgO in phase pure cubic form were synthesized using alkali leached hydrothermal method. The synergistic effect of particle size, morphology and doping of metal ions in nanocrystalline MgO was investigated for the Wittig reactions. Doping of Cu in MgO increases the number of basic sites but decreases the strength of this basic sites, while doping of Fe in MgO decreases both number and strength of basic sites on surface of MgO. Doping of Mn increases the number and strength of basic sites while Oxidation state of Mn in doped MgO plays an important role in order to enhance the catalytic activity. It is largely attributed to enhancement of surface basicity. The Mn doped MgO is found to be an efficient recyclable catalyst compared to its Fe and Cu doped counterparts in reported Wittig reaction for ethyl cinnmate preparation. One pot Wittig reaction is reported for Cu, Fe and Mn doped nanocrystalline MgO under the optimized reaction conditions of activation temperature, solvent and concentration of precursors. We believe that our methodology is unique in the context of high yield, recyclable and ecofriendly catalyst.

Declaration of Competing Interest

The authors declare that they have no known competing financial interests or personal relationships that could have appeared to influence the work reported in this paper.

Acknowledgement

Dr. Mansur Moulavi sincerely thanks to Dr. B. B. Kale - Director, C-MET (Pune), Dr. Sudhir Arbuj C-MET (Pune) for providing characterization facilities. The authors extend their appreciation to the Deanship of Scientific Research at King Saud University for funding this work through research group No (RG-1440-093).

References

Babaie, M., Sheibani, H., 2011. Nanosized magnesium oxide as a highly effective heterogeneous base catalysts for rapid synthesis of pyranopyrazole via a tandem four component reaction. Arab. J. Chem. 4 (2), 159–162.

Choudhari, B.M., Mahendar, K., Kantam, M.L., Ranganath, K., Athar, T., 2006. The one pot–Wittig reaction: a facile synthesis of α, β-unsaturated esters and nitriles by using nanocrystalline MgO. Adv. Synth. Catal. 348 (14), 1977–1985.

Coluccia, S., Tench, A.J., 1979. Surface structure and surface state and surface state in magnesium oxide powders. J. Chem. Soc. Faraday Trans. 1. 75(0), 1769–1779.

Corma, A., Iborra, S., 2006. Optimization of alkaline earth metal oxide and hydroxide catalysts for base catalyzed reactions. Adv. Catal. 49 (2006), 239–302.

Di Cosimo, J.I., Diez, V.K., Ferretti, C., Apesteguia, 2014. Basic catalysis on MgO: Generation, Characterization and catalytic properties of active sites. Catalysis 26(26), 1–28. Royal Society of Chemistry (Chapter 1).

Ding, Y., Zhang, G., Wu, H., Hai, B., Wang, L., Qian, Y., 2001. Nanoscale magnesium hydroxide and magnesium oxide powders: Control over size, shape, and structure via hydrothermal synthesis. Chem. Mater. 13 (2), 435–440.

Drexler, M.T., Amiridis, M.D., 2003. The effect of solvent on the heterogeneous synthesis of flavones over MgO. J. Catal. 214 (1), 136–145.

Fan, Y., Smith, K.J., Lupke, G., Hanbicki, A.T., Goswami, R., Li, C. H., Zhao, H.B., Jonkar, B.T., 2013. Exchang bias of the interface system at Fe/MgO interface. Nat. Nanotechnol. 8 (2013), 438–444.

Gadge, S.T., Mishra, A., Gajenji, A.L., Shahi, N.V., Bhanage, B.B., 2014. Magnesium oxide as a heterogeneous and recyclable base for the N-methylation of indole and o-methylation of phenol using dimethyl carbonate as a green methylating agent. RSC Adv. 4 (2014), 50271.

Gholinejad, M., Firouzabadi, H., Bahrami, M., Nájera, C., 2016. Tandem oxidation–Wittig reaction using nanocrystalline barium manganate (BaMnO4); an improved one-pot protocol. Tetrahedron Lett. 57, 3773–3775.

Gholinejad, M., Bahrami, M., Nájera, C., Biji Pullithadathil, B., 2018. Magnesium oxide supported bimetallic Pd/Cu nanoparticles as an efficient catalyst for Sonogashira reaction. J. Catal. 363, 81–91.

Hadia, N., Mohamed, H., 2015. Characteristics and optical properties of MgO nanowires synthesized by solvothermal method. Mater. Sci. Semicond. Process. 29 (2015), 238–244.

Hattori, H., 1995. Heterogeneous basic catalysis. Chem. Rev. 95 (3), 537–558.

Hattori, H., 2001. Solid base catalysts: Generation of basic sites and application to organic synthesis. Appl Catal A-Gen. 222 (1–2), 247–259.

Hattori, H., 2004. Solid base catalysis: Generation, Characterization and catalytic behavior of basic sites. J. Jpn. Pet. Inst. 47 (2), 67–81.

Kanade, K.G., Kale, B.B., Baeg, J., Lee, S.M., Lee, C.W., 2007. Self assembled aligned Cu doped ZnO for photocatalytic hydrogen production under visible light irradiation. Mater. Chem. Phys. 102 (1), 98–104.

Kanade, K.G., Baeg, J.O., Apte, S.K., Prakash, T.L., Kale, B.B., 2008. Synthesis and characterization of nanocrystalline zirconia by hydrothermal method. Mater. Res. Bull. 43 (3), 723–729.

Kantam, M.L., Pal, U., Sreedhar, B., Choudary, B.M., 2007. An efficient synthesis of organic carbonates using nanocrystalline magnesium oxide. Adv. Synth. Catal. 349 (2007), 1671–1675.

Kantam, M.L., Shiva Kumar, K.B., Balasubramanyam, V., Venkanna, G.T., Figueras, F., 2010. One pot Wittig reaction for the synthesis of α, β-unsaturated esters using highly basic magnesium/lanthanum mixed oxide. J. Mol. Catal. A: Chem. 321, 10–14.

Kunde, S.P., Kanade, K.G., Karale, K.B., Akolkar, H.N., Randhavanae, P.V., Shinde, S.T., 2016. Synthesis and characterization of nanostructured Cu-ZnO: An efficient catalysts for the preparation of (E)-3-styrylchromone. Arab. J. Chem. 12 (2019), 5212–5222.

Lee, D.W., Park, Y.M., Lee, K.Y., 2009. Heterogeneous Base Catalysts for Transesterification in Biodiesel Synthesis. Catal. Surv. Asia 13 (2009), 63–77.

Leng, L.C., Nandanan, E., Jackie, Y.Y., 2013. Nanostructured catalyst for organic transformations. Acc. Chem. Res. 46 (8), 1825–1837.

Lucrecia, A, Jesu's, H, Alberto, M, Jose M.M., Francisco J.U., 2016. Sustainable C-C bond formation through Knoenvengal reaction catalyzed by MgO-based catalysts. Reac. Kinet. Mech. 118(1), 247–265.

Mansour, A.N., Brizzolara, R.A., 1996. Characterization of the Surface of FeO Powder by XPS. Surf. Sci. Spectra 4 (1996), 345–350.

Menezes, O.A., Silva, P.S., Hernandez, E.P., Borges, L.E.P., Fraga, M. A., 2010. Tuning surface basic properties on nanocrystalline MgO by controlling preparation condition. Langmuir 26 (5), 3382–3387.

Moison, H., Taxier-Boullet, F., Foucad, A., 1987. Knoevenagel, Wittig and Wittig-Horner reactions in presence of magnesium oxide or zinc oxide. Tetrahedron 43 (3), 531–542.

Moulavi, M.H., Kale, B.B., Bankar, D., Amalnerkar, D.P., Vinu, A., Kanade, K.G., 2019. Green synthetic methodology: An evaluative study for impact of surface basicity of MnO2 doped MgO nanocomposites in Wittig reaction. J. Sol. St. Chem. 269, 167–174.

Nakhate, G.G., Nikam, V.S., Kanade, K.G., Arbuj, S., Kale, B.B., Baeg, J.O., 2010. Hydrothermally derived nano sized Ni doped TiO_2: A visible light driven photocatalysts for methylene blue degradation. Mater. Chem. Phys. 124 (2–3), 976–981.

Nesbitt, H.W., Banergee, D., 1998. Interpretation of XPS Mn(2p) spectra of Mn oxyhydroxides and constraints on the mechanism of MnO_2 precipitation. Am. Mineral. 83, 305–315.

Nicolaou, K.C., Harter, M.W., Gunzner, J.L., Nadin, A., 1997. The Wittig and related reactions in natural product synthesis. **Liebigs** Ann. 1997 (7), 1283–1301.

Philippt, R., Fujimoto, K., 1992. FTIR spectroscopic studies COP adsorption/Desorption on MgO/CaO catalysts. J. Phys. Chem. 96 (22), 9035–9038.

Pudi, S.M., Zoeb, A., Biswas, P., Kumar, S., 2015. Liquid phase conversion of glycerol to propanediol over highly active Copper/Magnesia catalysts. J. Chem. Sci. 127 (5), 833–842.

Raman, C.V., 1947. The vibration spectra of crystals-Part IV. Magnesium oxide. Proc. Indian Acad. Sci. A 26 (1947), 383–390.

Raman, C.V., 1961. The vibrations of MgO crystal structure and its infrared absorption spectrum. Proc. Indian Acad. Sci. A. 54 (1961), 205–222.

Shinde, S.T., Kanade, K.G., Karale, B.K., Amalnerkar, D.P., Thorat, N.M., Arbuj, S.S., Kunde, S.P., 2016. Nanosized ZnO under solvent free condition: A smart and ecofriendly catalyst to microwave assisted synthesis of 3,4-dihydropyromidin-2(1H)-ones/thiones. Curr. Smart Mater. 1 (1), 68–166.

Stavale, F., Shao, X., Nilius, N., Freund, H.J., Prada, S., Livia, G.M., Pacchioni, G., 2012. Donor characteristics of transition metal doped oxides: Cr doped MgO versus Mo doped CaO. J. Am. Chem. Soc. 134 (128), 11380–11383.

Stranick, M.A., 1999. MnO_2 by XPS Surf. Sci. Spectra 6 (1999), 31–38.

Taber, D.F., Nelson, C.G., 2006. Potassium hydride in paraffin: A useful base for organic synthesis. J. Org. Chem. 71 (23), 8973–8974.

Tanabe, K., Yamaguch, T., 1964. Basicity and acidity of solid surfaces. J. Res. Inst. Catal. Hokkaido Univ. 11 (3), 179–184.

Ueda, W., Yokoyama, T., Moro-oka, Y., Ikawa, T., 1985. Enhancement of surface base property of magnesium oxide by combination of metal ion. Chem. Lett. 14 (7), 1059–1062.

Vasquez, R.P., 1998. CuO by XPS. Surf. Sci. Spectra 5, 265–266.

Vedrine, J.C., 2015. Acid–base characterization of heterogeneous catalysts: an up-to-date overview. Res. Chem. Intermed. 41 (12), 9387–9423.

Wu, M.C., Goodman, D.Y., 1992. Acid/base properties of MgO studied by high energy resolution electron loss spectroscopy. Catal. Lett. 15 (1), 1–11.

Zhang, M., Gao, M., Chenab, J., Yu, Y., 2015a. Study on key step of 1,3-butadiene formation from ethanol on MgO/SiO_2. RSC Adv. 5 (33), 25959.

Zhang, J., Wu, Y., Li, L., Wang, X., Zhang, Q., Zhang, T., Tan, Y., Han, Y., 2016. Ti-SBA-15 supported Cu-MgO catalyst for synthesis of isobutyraldehyde from methanol and ethanol. RSC Adv. 6 (2016), 85940.

Zhang, X., Zheng, Y., Feng, X., Han, X., Bai, Z., Zhiping Zhang, Z., 2015b. Calcination temperature-dependent surface structure and physicochemical properties of magnesium oxide. RSC Adv. 5 (2015), 86102–185112.